Rotation of complex ions with ninefold hydrogen coordination studied by quasielastic neutron scattering and first-principles molecular dynamics calculations

Yoshinori Ohmasa,[1] Shigeyuki Takagi,[2] Kento Toshima,[2] Kaito Yokoyama,[2] Wataru Endo,[2] Shin-ichi Orimo,[2,3,*] Hiroyuki Saitoh,[4] Takeshi Yamada,[5] Yukinobu Kawakita,[6] Kazutaka Ikeda,[7,8,9] Toshiya Otomo,[7,8,9,10] Hiroshi Akiba,[1] and Osamu Yamamuro[1,†]

[1]*Institute for Solid State Physics, University of Tokyo, Kashiwa, Chiba 277-8581, Japan*
[2]*Institute for Materials Research, Tohoku University, Sendai 980-8577, Japan*
[3]*Advanced Institute for Materials Research (WPI-AIMR), Tohoku University, Sendai 980-8577, Japan*
[4]*Quantum Beam Science Directorate, National Institutes for Quantum Science and Technology, Hyogo 679-5148, Japan*
[5]*Neutron Science and Technology Center, Comprehensive Research Organization for Science and Society (CROSS), Tokai, Ibaraki 319-1106, Japan*
[6]*Neutron Science Section, Japan Proton Accelerator Research Complex (J-PARC), Japan Atomic Energy Agency, Tokai, Ibaraki 319-1195, Japan*
[7]*Institute of Materials Structure Science, High Energy Accelerator Research Organization (KEK), Tokai, Ibaraki 319-1106, Japan*
[8]*J-PARC Center, High Energy Accelerator Research Organization (KEK), Tokai, Ibaraki 319-1106, Japan*
[9]*School of High Energy Accelerator Science, The Graduate University for Advanced Studies, Tsukuba, Ibaraki 305-0801, Japan*
[10]*Graduate School of Science and Engineering, Ibaraki University, Tokai, Ibaraki 319-1106, Japan*

(Received 17 April 2022; accepted 15 August 2022; published 19 September 2022)

Quasielastic neutron scattering (QENS) and neutron powder diffraction of the complex transition metal hydrides Li_5MoH_{11} and Li_6NbH_{11} were measured in a temperature range of 10–300 K to study their structures and dynamics, especially the dynamics of the hydrogen atoms. These hydrides contain unusual ninefold H-coordinated complex ions (MoH_9^{3-} or NbH_9^{4-}) and hydride ions (H^-). A QENS signal appeared >150 K due to the relaxation of H atoms. The intermediate scattering functions derived from the QENS spectra are well fitted by a stretched exponential function called the Kohlrausch-Williams-Watts functions with a small stretching exponent $\beta \approx 0.3$–0.4, suggesting a wide relaxation time distribution. The Q dependence of the elastic incoherent structure factor is reproduced by the rotational diffusion of MH_9 (M = Mo or Nb) anions. The results are well supported by a van Hove analysis for the motion of H atoms obtained using first-principles molecular dynamics calculations. We conclude that the wide relaxation time distribution of the MH_9 rotation is due to the positional disorder of the surrounding Li ions and a unique rotation with MH_9 anion deformation (pseudorotation).

DOI: 10.1103/PhysRevResearch.4.033215

I. INTRODUCTION

The onset of an order-disorder phase transition with several orders of magnitude enhancement in ionic conductivity is often related to the rotational motion of polyanions in solid-state materials. The ion transport mechanism is referred to as the *paddle-wheel mechanism* [1–4] and has been extensively studied in the context of solid-state electrolytes for electrochemical devices, such as sensors, fuel cells, and batteries. The search for materials possessing such rotational polyanions has been intensive; representative families were identified, e.g., organic plastic crystals [5,6], sulfates [2,7], phosphates [8–10], and borohydrides [11,12]. The exploratory studies have been further stimulated by the discovery of the superior Li- or Na-ion transport properties in the series of closo-borane or closo-carborane salts [13–16].

A major drawback in this class of materials is their high phase transition temperatures and hence poor ionic conductivities at room temperature (RT), attributable to the high activation barrier for the rotational motion of polyanions. Several strategies have been proposed to overcome this drawback [4], such as crystallization from glassy precursors [17], chemical substitution [15,16,18], anion alloying [19–23], and crystallite-size reduction [24]; however, only a few materials can achieve RT superionic conduction based on these strategies [20,22,23].

Thus, we recently proposed an approach to suppress the phase transition temperature using homoleptic transition metal hydride complexes with high H coordination, wherein H is the sole ligand species, covalently binding to single transition metals [25–29], as a class of rotatable polyanions [30]. The motivation for this approach came from the fact that the rotational motion only requires displacements of H, which

*shin-ichi.orimo.a6@tohoku.ac.jp
†yamamuro@issp.u-tokyo.ac.jp

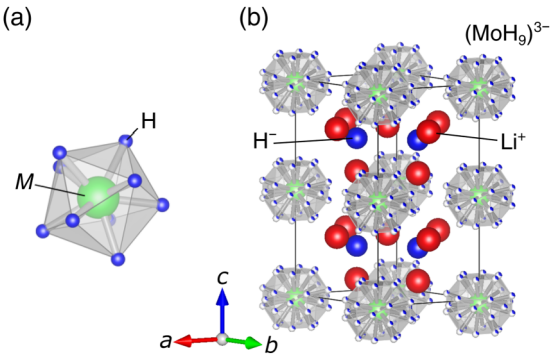

FIG. 1. (a) Tricapped trigonal prism structure of MH_9 (M = Mo, Nb, W, and Ta) clusters. (b) The structure of deuteride analog Li_5MoD_{11} obtained by neutron powder diffraction (NPD) [29].

is the lightest element with high mobility; hence, the displacements are expected to occur with low activation energy. An existing complex transition metal hydride Li_5MoH_{11} containing the ninefold H coordination hydride complex MoH_9^{3-} (Fig. 1) [29] was considered as an example to demonstrate this approach, and we found that MoH_9^{3-} exhibited not only conventional rigid-body rotation but also pseudorotation with an extremely low activation energy of a few millielectronvolts. The latter motion is essential because the resulting high degree of orientational disorder significantly enhances the entropic contribution to free energy, thereby stabilizing the disordered high-temperature (HT) phase. Moreover, our first-principles molecular dynamics (FPMD) calculations elucidated that the Li-ion conductivity in Li_5MoH_{11} reached $7.9 \times 10^{-2}\,S\,cm^{-1}$ at RT, >3 times greater than the highest RT Li-ion conductivity previously reported for $Li_{9.54}Si_{1.74}P_{1.44}S_{11.7}Cl_{0.3}$ ($2.5 \times 10^{-2}\,S\,cm^{-1}$) [31].

In this paper, we have performed neutron powder diffraction (NPD) and quasielastic neutron scattering (QENS) measurements of Li_5MoH_{11} and Li_6NbH_{11} to study their structures and dynamics, especially the dynamics of MH_9 (M = Mo or Nb) clusters. QENS is a robust method for analyzing materials containing H atoms because the scattering cross-section of an H atom, especially an incoherent one ($80.3 \times 10^{-24}\,cm^{-2}$), is much larger than those of other elements. In addition to the experiments, we theoretically studied the dynamics of the MH_9 clusters by analyzing the Fourier transform of the self-part of the van Hove correlation function, i.e., the intermediate scattering function (ISF), for the motion of H atoms simulated by FPMD calculations for Li_5MoH_{11}.

II. APPROACH

A. Experimental

Li_5MoH_{11} and Li_6NbH_{11} samples were prepared using a high-pressure and HT technique reported elsewhere [29]. Powdered mixtures of LiH and Mo or Nb metals were hydrogenated under 5 GPa at 923–1023 K for 24–48 h. The synthetic conditions were determined via *in situ* synchrotron radiation x-ray diffraction measurements at the beamline BL14B1, SPring-8 [32].

To check the number of impurities in the samples, NPD experiments were performed using a time-of-flight (TOF)-type high-intensity total diffractometer NOVA, which is installed at BL21, Materials and Life Science Experimental Facility (MLF), Japan Proton Accelerator Research Complex (J-PARC). The samples were loaded in a cylindrical vanadium container with 3-mm diameter. The amount of the samples was ~31 and 13.5 mg for Li_5MoH_{11} and Li_6NbH_{11}, respectively. The diffraction patterns were recorded at RT. The measurement time was ~24 h for both samples. The data were analyzed by the Rietveld fitting method using the Z-code software [33].

QENS data were collected using a TOF-type near-backscattering spectrometer DNA installed at BL02, MLF, J-PARC. We used two resolution modes, which can be switched by a pulse-shaping chopper: one is the high-resolution (HR) mode whose energy resolution was ~3 μeV and energy window was $-40\,\mu eV < E < 100\,\mu eV$, and the other is the low-resolution (LR) mode whose energy resolution was ~15 μeV and energy window was $-500\,\mu eV < E < 1500\,\mu eV$. The momentum transfer range was $0.13 Å^{-1} < Q < 1.98\,Å^{-1}$ for both modes. The intensity of the LR mode was >10 times greater than that of the HR mode. The samples were loaded in a concentric double-cylindrical aluminum cell, with a 14-mm inner diameter of the outer cylinder and a 0.5-mm sample thickness. The amount of the samples was 33 and 20 mg for Li_5MoH_{11} and Li_6NbH_{11}, respectively. At the beginning of the measurements, we performed a fixed-window scan from 10 to 300 K in which the intensity of the elastic scattering was measured as a function of temperature with the HR mode. The QENS data for the Li_5MoH_{11} sample were measured at temperatures of 10, 150, 180, 210, 240, 270, and 300 K using the HR and LR modes, whereas those for the Li_6NbH_{11} sample were measured at 10, 150, 210, 240, 270, and 300 K using the LR mode and at 10, 240, 270, and 300 K using the HR mode. The spectra measured at 10 K are used as the instrumental resolution functions. The measurement times for the Li_5MoH_{11} sample were 7–10 and 7–8 h for the HR and LR modes, respectively, whereas those for the Li_6NbH_{11} sample were 19–23 and 6–7 h for the HR and LR modes, respectively. These measurement times are much longer than usual because the sample amounts were minute.

B. Computational

The theoretical ISF $I(Q, t)$ for the motion of nine H atoms in the MoH_9 clusters of Li_5MoH_{11} at 573, 673, 773, 873, and 973 K was evaluated using the following equation:

$$I(Q,t) = \left\langle \frac{\sin Q\Delta r(t)}{Q\Delta r(t)} \right\rangle, \quad (1)$$

where Q denotes the momentum transfer, and $\Delta r(t)$ denotes the displacements of nine H atoms of the MoH_9 clusters in Li_5MoH_{11} during time interval t. We employed the same FPMD trajectories as used to demonstrate the RT Li superionic conduction of this material in Ref. [30]. The motivation for this choice is to provide not only theoretical support for the present experimental results but also experimental support for the conclusion of Ref. [30].

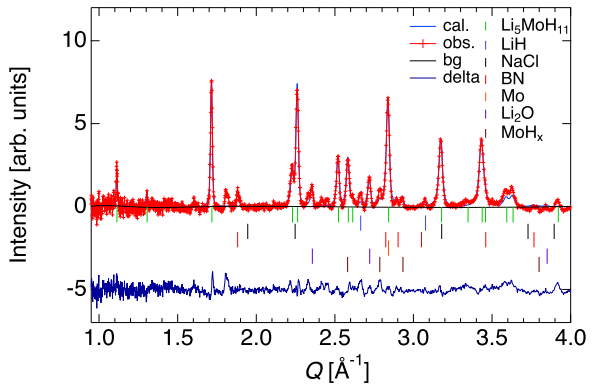

FIG. 2. The neutron powder diffraction (NPD) pattern of Li_5MoH_{11}. The solid curves in the upper portion are the Rietveld fitting (blue) and background (black) curves, and the solid curve in the lower portion is the difference between the observed and calculated intensities. The positions of the diffraction peaks for various components in the sample are indicated by the tick marks.

III. RESULTS AND DISCUSSION

A. NPD

Figures 2 and 3 show the observed and calculated NPD patterns of the Li_5MoH_{11} and Li_6NbH_{11} samples, respectively. The Rietveld analysis clarified that both samples, especially the Li_6NbH_{11} sample, contain considerable numbers of impurities. The diffraction patterns from the main components Li_5MoH_{11} and Li_6NbH_{11} are consistent with the hexagonal structure predicted by the first-principles calculations [29]. The structure model used for Li_5MoH_{11} has the space group $P6/mmm$ (No.191) and the lattice parameters $a = 5.551$ Å and $c = 5.631$ Å; meanwhile, the structure model for Li_6NbH_{11} has the space group $P6_3cm$ (No.185) and the lattice parameters $a = 5.457$ Å and $c = 12.09$ Å. The reliability of the Rietveld fitting was as follows: Li_5MoH_{11}: $R_{wp} = 18.9\%$, $S = 2.01$; Li_6NbH_{11}: $R_{wp} = 29.6\%$, $S = 1.65$.

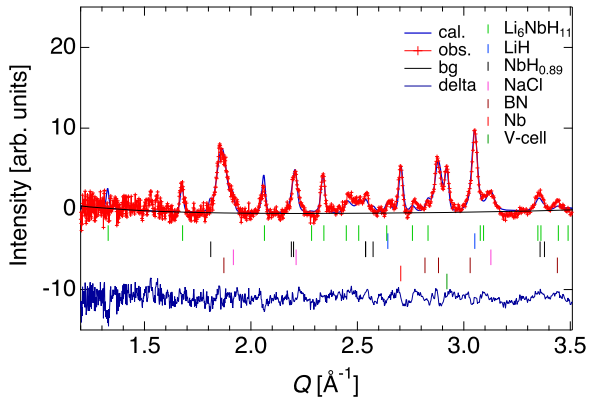

FIG. 3. The neutron powder diffraction (NPD) pattern of Li_6NbH_{11}. The solid curves in the upper portion are the Rietveld fitting (blue) and background (black) curves, and the solid curve in the lower portion is the difference between the observed and calculated intensities. The positions of the diffraction peaks for various components in the sample are indicated by the tick marks.

TABLE I. The mass fraction of each component in Li_5MoH_{11} estimated from the Rietveld analysis and the corresponding fraction of H atoms.

	Mass fraction	H-atom fraction
Li_5MoH_{11}	0.752	0.851
Mo	0.134	
LiH	0.081	0.148
Li_2O	0.016	
MoH_x	0.014	0.001
BN	0.002	
NaCl	0.000	

The mass fractions of each component in the Li_5MoH_{11} and Li_6NbH_{11} samples estimated from the Rietveld analysis are listed in Tables I and II, respectively. The corresponding H-atom fractions are also listed in the tables. Although the overall NPD profile is well fitted by the model calculation, some peaks remain unexplained. Therefore, there are still some uncertainties in the estimation of the component fraction. Thus, the NPD experiments confirmed that the QENS spectra were mainly from the H atoms in Li_5MoH_{11} or Li_6NbH_{11} because most H atoms belong to Li_5MoH_{11} or Li_6NbH_{11}. The influence of H atoms in the impurities on the QENS spectra will be discussed later.

B. QENS

Figure 4 shows the results of the fixed-window scans of Li_5MoH_{11} and Li_6NbH_{11}. For both samples, the intensity of the elastic scattering was nearly constant <150 K. Above 150 K, the elastic intensity decreased on heating, indicating that the motion of H atoms in both samples is activated on the time scale of the HR mode of DNA (∼1 ns). Figures 5 and 6 show the dynamic structure factors $S(Q, E)$ of Li_5MoH_{11} and Li_6NbH_{11}, respectively. Peak broadening due to QENS was observed in both HR and LR data. The statistical accuracy of Li_5MoH_{11} data was much better than that of Li_6NbH_{11} data because the Li_5MoH_{11} sample had a larger amount and less impurity. When the temperature was increased, the intensity and width of the QENS component increased. It is unusual that the QENS component is observed in such a wide temperature range in both HR and LR mode data.

We calculated the ISF $I(Q, t)$ by Fourier transforming $S(Q, E)$ with respect to E. As shown in Fig. 7(a), the data at 300 K indicate that the relaxation occurs in almost three

TABLE II. The mass fraction of the components in Li_6NbH_{11} estimated from the Rietveld analysis and the corresponding fraction of H atoms.

	Mass fraction	Fraction of H atoms
Li_6NbH_{11}	0.570	0.840
BN	0.258	
LiH	0.064	0.157
Nb	0.051	
NaCl	0.040	
$NbH_{0.89}$	0.017	0.003

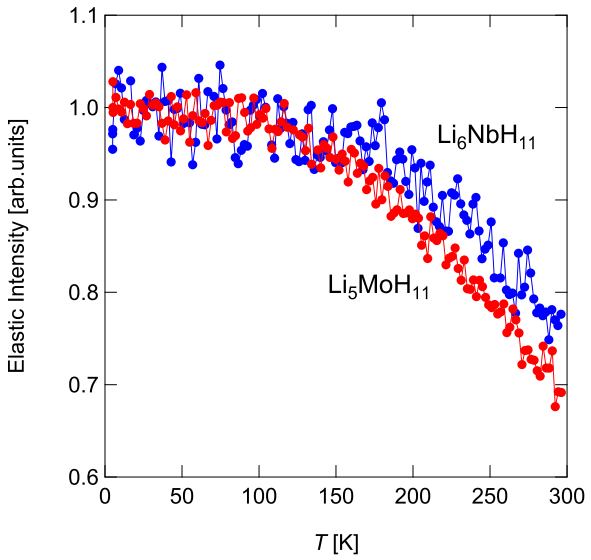

FIG. 4. Results of fixed-window scan for Li_5MoH_{11} and Li_6NbH_{11} at $Q = 1.15\,Å^{-1}$.

orders of magnitude (from 1 to 1000 ps). This wide relaxation cannot be reproduced by a single exponential function. Hence, we fitted the data using a stretched exponential function called the Kohlrausch-Williams-Watts (KWW) function [34,35]:

$$I(Q,t) = a(Q) + b(Q)\exp\left[-\left(\frac{t}{\tau_{\mathrm{KWW}}}\right)^{\beta}\right], \qquad (2)$$

where β denotes the stretching exponent, indicating the width of the relaxation time spectrum [36] (the width increases as β decreases); τ_{KWW} denotes the characteristic relaxation time; and $a(Q)$ and $b(Q)$ represent the intensities of the elastic and quasielastic components, respectively. In this equation, the elastic incoherent structure factor (EISF) is expressed as $a(Q)/[a(Q) + b(Q)]$. The solid curves in Fig. 7(a) represent the fitting curves. To make the fitting with good convergence and obtain reliable parameters, we tried reducing the number of fitting (flexible) parameters. First, we assumed that the EISF does not depend on T. This means that the number of mobile H atoms and the shape of their moving region do not change with T. This assumption should be valid if QENS is ascribed to the reorientational motion of MH_9 clusters. We adopted the common EISF calculated from the data at $T = 300$ K, where the overall feature of the relaxation was obtained. In the lower temperature region, however, a part of the relaxation with longer relaxation times is out of the observable window, and so it is impossible to obtain the EISF only from the experimental data. We also assumed that τ_{KWW} and β do not depend on Q. Equation (2) fits the experimental data well, as indicated by the solid lines in Fig. 7(a). The determined β ($\approx$0.3–0.4) shown by the red circles in Fig. 8 was quite small, indicating that the relaxation time had a large distribution, which agreed with the fact that the quasielastic component of $S(Q,E)$ was observed in the very wide temperature range in both HR and LR mode data (Figs. 5 and 6); i.e., a part of the widely distributing relaxation time remained in the window of observation, even if the mean relaxation time was changed with temperature.

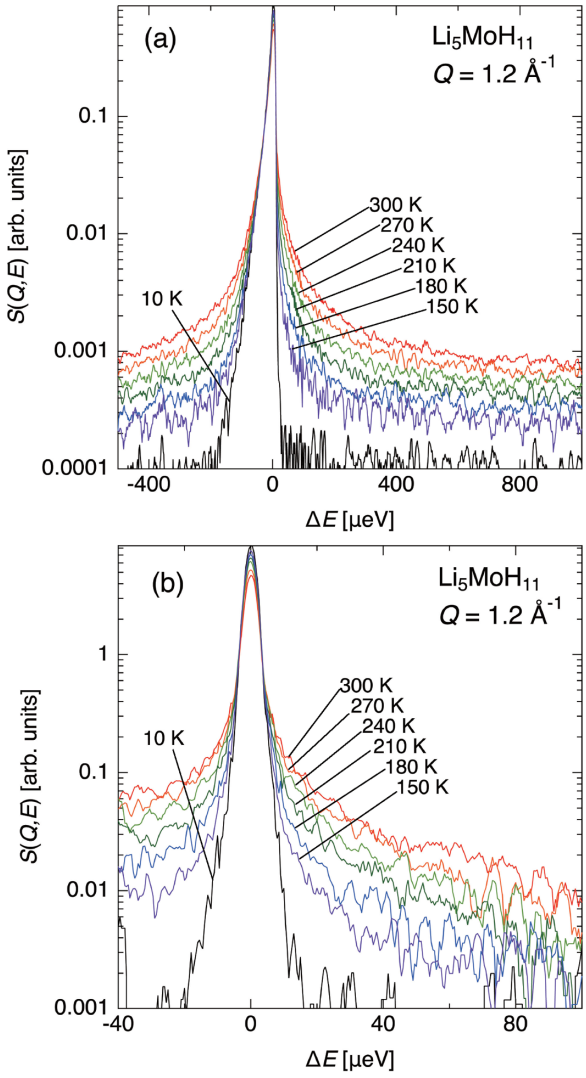

FIG. 5. Quasielastic neutron scattering (QENS) spectra of Li_5MoH_{11} measured in (a) low-resolution (LR) and (b) high-resolution (HR) modes at various temperatures at $Q = 1.2\,Å^{-1}$.

Similar relaxation behavior was observed for the motion of H atoms in the FPMD calculations for Li_5MoH_{11}: the theoretically obtained ISF $I(Q,t)$ is also well fitted to Eq. (2) [Fig. 7(b)]. The green triangles in Fig. 8 show β from FPMD calculations. Remarkably, the experiments and the FPMD calculations can be joined smoothly, as shown by the dotted line. It is a general trend that β decreases in the lower temperature region [37]. Notably, no assumption was made in the KWW fits of the theoretically obtained $I(Q,t)$.

We also analyzed the ISF $I(Q,t)$ for the Li_6NbH_{11} sample (Fig. 9). The symbols represent the experimental $I(Q,t)$, and the solid lines represent the fitting curves by Eq. (2). In this calculation, we used common EISF and β parameters obtained from the data at 300 K. The overall feature of the experimental data is well reproduced by the fitting curves with the stretching exponent $\beta = 0.33$, although the counting statistics of the experimental data are poorer than that of the Li_5MoH_{11} data.

The fact that $I(Q,t)$ is well fitted using Q-independent τ_{KWW} suggests that the relaxation is a localized mode, such

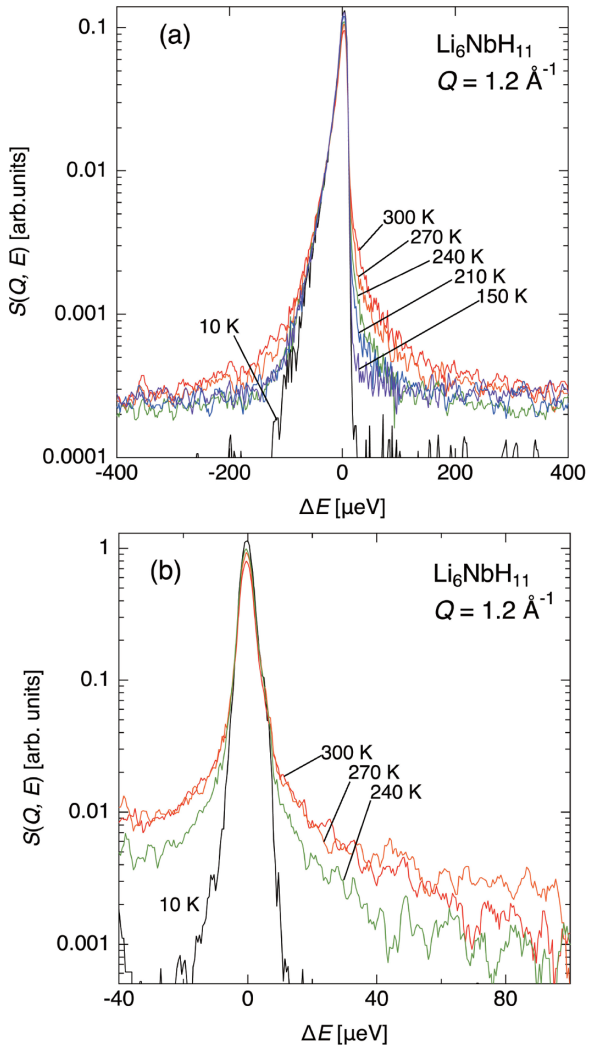

FIG. 6. Quasielastic neutron scattering (QENS) spectra of Li_6NbH_{11} measured in (a) low-resolution (LR) and (b) high-resolution (HR) modes at various temperatures at $Q = 1.2$ Å^{-1}.

as a reorientational motion of the clusters. As temperature decreases, τ_{KWW} increases, indicating that the relaxation is a thermal excitation process. Figure 10 shows the Arrhenius plots of τ_{KWW} for the Li_5MoH_{11} and Li_6NbH_{11} samples, as well as the motion of H atoms in the FPMD calculations for Li_5MoH_{11}. It is plausible that the extrapolations of the experimental and calculated points merge smoothly. The activation energies obtained from the slopes of the plots were 15.8 ± 0.8 and 27 ± 4 kJ/mol for Li_5MoH_{11} and Li_6NbH_{11}, respectively, whereas an activation energy of 14.7 ± 1.1 kJ/mol was obtained from the FPMD calculations for Li_5MoH_{11}. These values are like those of other cluster materials. For example, the reorientational motion of the $B_{12}H_{12}$ cluster in the superionic conducting phase of $Na_2B_{12}H$ has an activation energy of 25 kJ/mol [38], and those of the BH_4 cluster in the HT phase of $NaBH_4$ and KBH_4 are 11.9 ± 0.5 and 14.6 ± 0.5 kJ/mol, respectively [39]. The activation energy of Li_6NbH_{11} is larger than that of Li_5MoH_{11}, attributable to the difference in the electric charge of the clusters $(NbH_9)^{4-}$ and $(MoH_9)^{3-}$; the potential barrier due to the Coulomb interaction of $(NbH_9)^{4-}$ may be greater than that of $(MoH_9)^{3-}$.

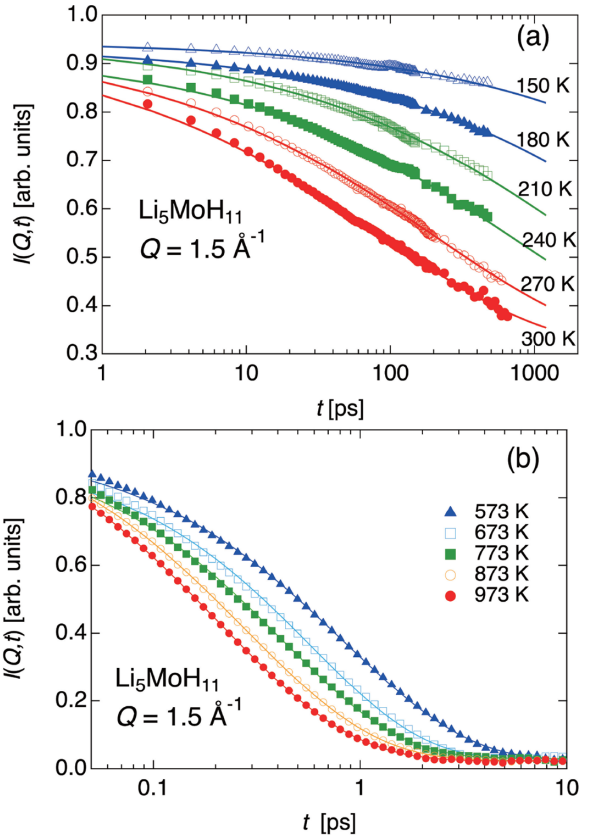

FIG. 7. Intermediate scattering function (ISF) $I(Q, t)$ for Li_5MoH_{11} at $Q = 1.5$ Å^{-1} obtained from (a) quasielastic neutron scattering (QENS) data and (b) first-principles molecular dynamics (FPMD) calculations. The solid lines represent fitting curves to the Kohlrausch-Williams-Watts (KWW) function.

The solid circles and squares in Fig. 11(a) indicate the EISF at 300 K for the Li_5MoH_{11} and Li_6NbH_{11} samples, respectively. The EISF data for both samples show a gradual decrease from 1 as Q increases and tend to saturate to nonzero values at the high-Q limit. A similar trend was observed for the EISF estimated from the FPMD calculations for Li_5MoH_{11} at $T = 973$ and 573 K, as shown by the solid circles in Fig. 11(b). In the EISF calculation from FPMD, only the H atoms in the MoH_9 clusters were considered. These results coincide with characteristic features of local motions,

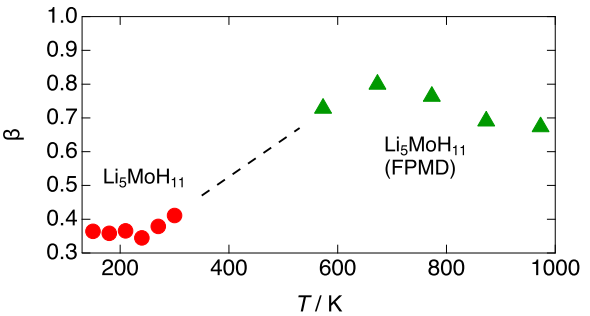

FIG. 8. Temperature dependence of the stretching exponent β of Li_5MoH_{11} (red circles) and that from first-principles molecular dynamics (FPMD) calculation (green triangles).

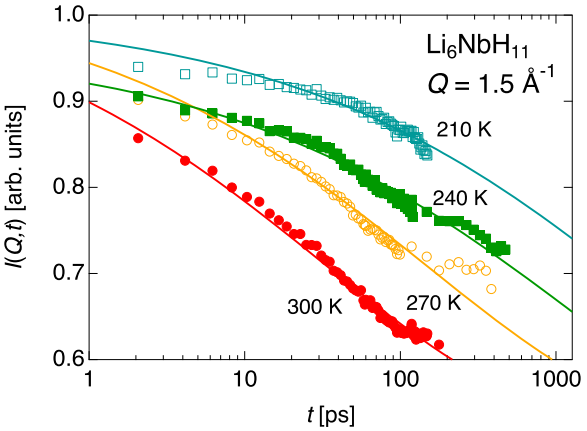

FIG. 9. The intermediate scattering function (ISF) of Li_6NbH_{11} at $Q = 1.5$ Å^{-1} and various temperatures. The symbols indicate the experimental data, and the solid curves are calculated from the Kohlrausch-Williams-Watts (KWW) function with $\beta = 0.33$.

such as rotations. We found that the EISF obtained from FPMD calculations changes only a little with temperature, justifying our assumption that the EISF does not depend on temperature. In this paper, we assumed the cluster rotation and tentatively analyzed the EISF data using the following equation:

$$\mathrm{EISF} = 1 - A + A j_0^2(QR), \tag{3}$$

where A and R (radius of the rotation) are constants, $j_0(QR)$ represents the spherical Bessel function of the zeroth order, and $1 - A$ represents the elastic scattering component from nonmoving H atoms contained in the sample. The nonmoving H atoms have two origins: one is the isolated H^- atoms located at the interstitial sites between clusters, and the other is the H atoms contained in the impurities. Of course, both origins may be valid. Moreover, $A j_0^2(QR)$ in Eq. (3) is the contribution from H atoms in clusters under the reorientational motion. In this paper, we adopted the isotropic rotational diffusion model [40,41]. In this model, H atoms in clusters are considered to diffuse continuously on a sphere with a radius R.

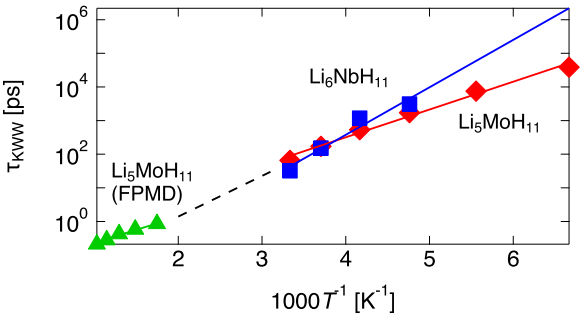

FIG. 10. Arrhenius plot for the characteristic relaxation time τ_{KWW} obtained from the quasielastic neutron scattering (QENS) data for Li_5MoH_{11} (red) and Li_6NbH_{11} (blue) as well as the first-principles molecular dynamics (FPMD) calculations for Li_5MoH_{11} (green).

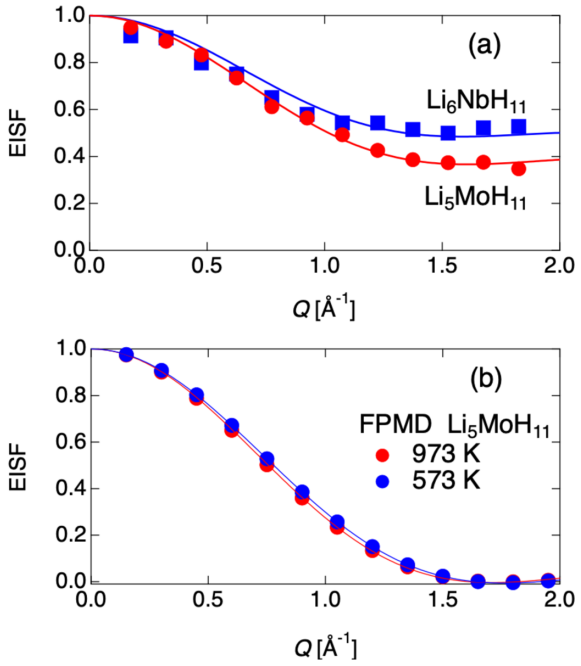

FIG. 11. Elastic incoherent structure factor obtained from (a) quasielastic neutron scattering (QENS) data for Li_5MoH_{11} and Li_6NbH_{11} at 300 K and (b) first-principles molecular dynamics (FMPD) calculations for H-atoms in MoH_9 clusters in Li_5MoH_{11} at 973 and 573 K. The solid circles and squares are experimental data. The solid curves are fitted to Eq. (3).

The solid lines in Fig. 11(a) are the curves fitted to Eq. (3). In this calculation, A and R are considered free parameters. The overall feature of the EISF for both samples is well explained by this model. The obtained fitting parameters are $A = 0.63$ and $R = 1.96$ Å for Li_5MoH_{11} and $A = 0.49$ and $R = 2.35$ Å for Li_6NbH_{11}. The R values are close to the radius of the clusters 1.74–1.78 Å for Li_5MoH_{11} and 1.84–1.88 Å for Li_6NbH_{11}, which were obtained from the first-principles calculations at 0 K [29]. This result suggests that the relaxation is due to the cluster rotation. The experimental R are 10–20% greater than the calculated values, probably because the center of the rotation is moving. This situation might occur for clusters with lower symmetry.

This is theoretically supported by the fact that the EISF data estimated from the FPMD calculations for Li_5MoH_{11}, where the H atoms exhibit spherical distribution with a slight localization along the specific directions as shown in Fig. 12, could also be well fitted to Eq. (3) with the fitting parameters $A = 1.00$ and $R = 1.78$ Å for 573 K.

If the nonzero term $1 - A$ in Eq. (3) is due to the H atoms at interstitial sites and in impurities, A is related to the fraction of the H atoms in the impurities x as $A = (\frac{9}{11})(1 - x)$ because the fraction of the H atoms in the clusters is $\frac{9}{11}$ in the Li_5MoH_{11} and Li_6NbH_{11} crystals. In the present case, x was estimated to be 0.23 and 0.40 for Li_5MoH_{11} and Li_6NbH_{11}, respectively. These values are much greater than those obtained from the NPD data listed in Tables I and II. Another possible explanation for the discrepancy is that the diffusion of an H atom on a sphere is not continuous but jump diffusion. If the H atoms jump among N sites on the sphere, an additional contribution

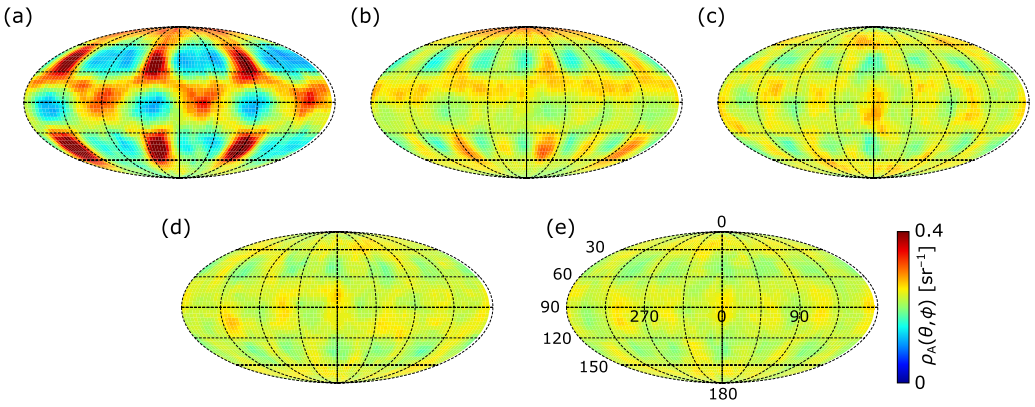

FIG. 12. Angular distribution of nine H atoms in MoH_9 estimated from the first-principles molecular dynamics (FPMD) calculations for Li_5MoH_{11} at (a) 573 K, (b) 673 K, (c) 773 K, (d) 873 K, and (e) 973 K. The origin is at the center of inertia of the MoH_9 unit at each FPMD time step, and the polar axis is along the c axis. The lower the temperature, the more pronounced the localization of the H atoms along the specific directions and the more dominant the cluster jump diffusion.

$(\frac{9}{11})(1-x)/N$ should be added to the elastic term. Indeed, as shown in Fig. 12, a weak site preference on the sphere suggesting the jump diffusion of H was observed in the FPMD calculations for Li_5MoH_{11} at elevated temperatures. Notably, such a site preference should be more pronounced in the LT region. Unfortunately, the current experimental data are insufficient to distinguish the two possibilities and specify more details about the rotational motion. To conclude whether the diffusion is continuous or jump diffusion, high-quality QENS data are required in higher Q and E regions.

Another question is the origin of the small stretching exponent β of 0.3–0.4. One possible explanation is that the reorientational motion of the clusters is strongly affected by the randomness of the Li-ion positions surrounding the clusters. As the rate of the cluster rotation is much faster than that of the Li jumps, the clusters may feel different potential fields corresponding to various Li position configurations. This situation yields the relaxation time distribution of the cluster reorientation. In addition to the positional disorder of Li ions, the reorientational motion of the clusters itself may be responsible for the wide relaxation time distribution. As reported in our previous paper [30], the MH_9 clusters undergo a unique rotation, called *pseudorotation*. In this motion, the clusters are continuously deformed via multiple metastable H-coordination modes to minimize the activation energy for their reorientation depending on the surrounding environment. Because the H positions in the clusters are primarily dominated by the ligand field symmetry, the fluctuation in the molecular geometry of the clusters by pseudorotation should significantly affect the potential energy for the H motion, thereby yielding the wide relaxation time distribution. In any case, our van Hove analysis using the FPMD trajectories [30] reproduces well the experimental QENS data; as such, the present combined experimental and theoretical study validates the mechanism of the RT Li superionic conduction discussed in Ref. [30].

IV. CONCLUSIONS

We performed NPD and QENS measurements for Li_5MoH_{11} and Li_6NbH_{11}, which contain unusual ninefold H-coordinated clusters MoH_9 and NbH_9. The NPD patterns agreed with the hexagonal structure predicted by the FPMD calculations in which the MoH_9 and NbH_9 clusters were orientationally disordered. The results of the fixed-window scan of QENS indicate that the motion of H atoms is activated >150 K on the time scale of nanoseconds. The ISFs obtained from the QENS spectra are well fitted by the KWW function with a very small stretching exponent ($\beta \approx 0.3$–0.4), indicating a wide relaxation time distribution. From the temperature dependence of the mean relaxation time, the activation energies are obtained to be 15.8 ± 0.8 and 27 ± 4 kJ/mol for Li_5MoH_{11} and Li_6NbH_{11}, respectively. The Q dependence of the EISF is explained by the rotational diffusion of H atoms on the clusters. All experimental results are well reproduced by the van Hove analysis using the FPMD calculation results.

ACKNOWLEDGMENTS

We are grateful for technical support from N. Warifune. The experiment in the MLF at J-PARC was performed with the approval of J-PARC (Proposals No. 2019A0250, No. 2019A0298, No. 2020A0149, and No. 2020A0251). The FPMD calculations were done using MASAMUNE-IMR (MAterials science Supercomputing system for Advanced MUlti-scale simulations towards NExt-generation - Institute for Materials Research). (Project No. 2012SC0406). The synthetic conditions of the samples were determined by *in situ* synchrotron radiation-based x-ray diffraction measurements at the beamline BL14B1 SPring-8, with the approval of the Japan Synchrotron Radiation Research Institute (Proposals No. 2017B3680, No. 2018A3680, No. 2018B3680, No. 2019A3680, No. 2019B3680, and No. 2020A3680) and the QST under the remit of "Nanotechnology Platform" of the Ministry of Education, Culture, Sports, Science and Technology (MEXT), Japan (Proposals No. JPMXP09A17QS0023, No. JPMXP09A18QS0012, No. JPMXP09A18Q0033, No. JPMXP09A19QS0012, No. JPMXP09A19QS0033, and No. JPMXP09A20QS0015). This paper is financially supported by JSPS KAKENHI No. JP18H05513 and No. JP18H05518 (Hydrogenomics) and No. JP19H05514 and No. 20K20438.

Y.O. and S.T. contributed equally to this paper.

[1] A. Lundén, Enhancement of cation mobility in some sulphate phases due to a paddle-wheel mechanism, Solid State Ion. **28**, 163 (1988).

[2] A. Lundén, Evidence for and against the paddle-wheel mechanism of ion transport in superionic sulphate phases, Solid State Commun. **65**, 1237 (1988).

[3] Z. Zhang, P.-N. Roy, H. Li, M. Avdeev, and L. F. Nazar, Coupled cation-anion dynamics enhances cation mobility in room-temperature superionic solid-state electrolytes, J. Am. Chem. Soc. **141**, 19360 (2019).

[4] Z. Zhang and L. F. Nazar, Exploiting the paddle-wheel mechanism for the design of fast ion conductors, Nat. Rev. Mater. **7**, 389 (2022).

[5] D. R. MacFarlane, P. Meakin, N. Amini, and M. Forsyth, Structural studies of ambient temperature plastic crystal ion conductors, J. Phys. Condens. Matter. **13**, 8257 (2001).

[6] D. R. MacFarlane and M. Forsyth, Plastic crystal electrolyte materials: New perspectives on solid state ionics, Adv. Mater. **13**, 957 (2001).

[7] R. Aronsson, B. Jansson, H. E. G. Knape, A. Lundén, L. Nilsson, C.-A. Sjöblom, and L. M. Torell, Fast ion conductors with rotating sulphate ions, J. Phys. Colloq. **41**, C6 (1980).

[8] V. D. Wiench and M. Jansen, Über Na_3PO_4: Versuche zur Reindarstellung, Kristallstruktur der Hochtemperaturform, Z. Anorg. Allg. Chem. **461**, 101 (1980).

[9] J.-F. Brice, B. Majidi, and H. Kessler, Contribution a l'etude de la conductivite ionique de l'orthophosphate Na_3PO_4, Mater. Res. Bull. **17**, 143 (1982).

[10] M. Jansen, Volume effect or paddle-wheel mechanism–fast alkali-metal ionic conduction in solids with rotationally disordered complex anions, Angew. Chem. Int. Ed. **30**, 1547 (1991).

[11] M. Matsuo, Y. Nakamori, S. Orimo, H. Maekawa, and H. Takamura, Lithium superionic conduction in lithium borohydride accompanied by structural transition, Appl. Phys. Lett. **91**, 224103 (2007).

[12] M. Matsuo and S. Orimo, Lithium fast-ionic conduction in complex hydrides: Review and prospects, Adv. Energy Mater. **1**, 161 (2011).

[13] T. J. Udovic, M. Matsuo, A. Unemoto, N. Verdal, V. Stavila, A. V. Skripov, J. J. Rush, H. Takamura, and S. Orimo, Sodium superionic conduction in $Na_2B_{12}H$, Chem. Commun. **50**, 3750 (2014).

[14] T. J. Udovic, M. Matsuo, W. S. Tang, H. Wu, V. Stavila, A. V. Soloninin, R. V. Skoryunov, O. A. Babanova, A. V. Skripov, J. J. Rush *et al.*, Exceptional superionic conductivity in disordered sodium decahydro-closo-decaborate, Adv. Mater. **26**, 7622 (2014).

[15] W. S. Tang, A. Unemoto, W. Zhou, V. Stavila, M. Matsuo, H. Wu, S. Orimo, and T. J. Udovic, Unparalleled lithium and sodium superionic conduction in solid electrolytes with large monovalent cage-like anions, Energy Environ. Sci. **8**, 3637 (2015).

[16] W. S. Tang, M. Matsuo, H. Wu, V. Stavila, W. Zhou, A. A. Talin, A. V. Soloninin, R. V. Skoryunov, O. A. Babanova, A. V. Skripov *et al.*, Liquid-like ionic conduction in solid lithium and sodium monocarba-closo-decaborates near or at room temperature, Adv. Energy Mater. **6**, 1502237 (2016).

[17] A. Hayashi, K. Noi, A. Sakuda, and M. Tatsumisago, Superionic glass-ceramic electrolytes for room-temperature rechargeable sodium batteries, Nat. Commun. **3**, 856 (2012).

[18] Z. Zhang, H. Li, K. Kaup, L. Zhou, P.-N. Roy, and L. F. Nazar, Targeting superionic conductivity by turning on anion rotation at room temperature in fast ion conductors, Matter **2**, 1667 (2020).

[19] M. Matsuo, S. Kuromoto, T. Sato, H. Oguchi, H. Takamura, and S. Orimo, Sodium ionic conduction in complex hydrides with $[BH_4]^-$ and $[NH_2]^-$ anions, Appl. Phys. Lett. **100**, 203904 (2012).

[20] W. S. Tang, K. Yoshida, A. V. Soloninin, R. V. Skoryunov, O. A. Babanova, A. V. Skripov, M. Dimitrievska, V. Stavila, S. Orimo, and T. J. Udovic, Stabilizing superionic-conducting structures via mixed-anion solid solutions of monocarba-closo-borate salts, ACS Energy Lett. **1**, 659 (2016).

[21] K. Yoshida, T. Sato, A. Unemoto, M. Matsuo, T. Ikeshoji, T. J. Udovic, and S. Orimo, Fast sodium ionic conduction in $Na_2B_{10}H$–$Na_2B_{12}H$ pseudo-binary complex hydride and application to a bulk-type all-solid-state battery, Appl. Phys. Lett. **110**, 103901 (2017).

[22] S. Kim, H. Oguchi, N. Toyama, T. Sato, S. Takagi, T. Otomo, D. Arunkumar, N. Kuwata, J. Kawamura, and S. Orimo, A complex hydride lithium superionic conductor for high-energy-density all-solid-state lithium metal batteries, Nat. Commun. **10**, 1081 (2019).

[23] Y. Sun, Y. Wang, X. Liang, Y. Xia, L. Peng, H. Jia, H. Li, L. Bai, J. Feng, H. Jiang *et al.*, Rotational cluster anion enabling superionic conductivity in sodium-rich antiperovskite Na_3OBH_4, J. Am. Chem. Soc. **141**, 5640 (2019).

[24] W. S. Tang, M. Matsuo, H. Wu, V. Stavila, A. Unemoto, S. Orimo, and T. J. Udovic, Stabilizing lithium and sodium fast-ion conduction in solid polyhedral-borate salts at device-relevant temperatures, Energy Storage Mater. **4**, 79 (2016).

[25] K. Yvon, Complex transition metal hydrides, Chimia **52**, 613 (1998).

[26] H. Saitoh, S. Takagi, M. Matsuo, Y. Iijima, N. Endo, K. Aoki, and S. Orimo, Li_4FeH_6: Iron-containing complex hydride with high gravimetric hydrogen density, APL Mater. **2**, 076103 (2014).

[27] S. Takagi and S. Orimo, Recent progress in hydrogenrich materials from the perspective of bonding flexibility of hydrogen, Scripta Mater. **109**, 1 (2015).

[28] S. Takagi, Y. Iijima, T. Sato, H. Saitoh, K. Ikeda, T. Otomo, K. Miwa, T. Ikeshoji, K. Aoki, and S. Orimo, True boundary for the formation of homoleptic transition-metal hydride complexes, Angew. Chem. Int. Ed. **54**, 5650 (2015).

[29] S. Takagi, Y. Iijima, T. Sato, H. Saitoh, K. Ikeda, T. Otomo, K. Miwa, T. Ikeshoji, and S. Orimo, Formation of novel transition metal hydride complexes with ninefold hydrogen coordination, Sci. Rep. **7**, 44253 (2017).

[30] S. Takagi, T. Ikeshoji, T. Sato, and S. Orimo, Pseudorotating hydride complexes with high hydrogen coordination: A class of rotatable polyanions in solid matter, Appl. Phys. Lett. **116**, 173901 (2020).

[31] Y. Kato, S. Hori, T. Saito, K. Suzuki, M. Hirayama, A. Mitsui, M. Yonemura, H. Iba, and R. Kanno, High-power all-solid-state batteries using sulfide superionic conductors, Nat. Energy **1**, 16030 (2016).

[32] W. Utsumi, K. Funakoshi, Y. Katayama, M. Yamakata, T. Okada, and O. Shimomura, High-pressure science with a

multi-anvil apparatus at SPring-8, J. Phys. Condens. Matter **14**, 10497 (2002).

[33] R. Oishi, M. Yonemura, Y. Nishimaki, S. Torii, A. Hoshikawa, T. Ishigaki, T. Morishima, K. Mori, and T. Kamiyama, Rietveld analysis software for J-PARC, Nucl. Instrum. Methods Phys. Res. A **600**, 94 (2009).

[34] R. Kohlrausch, Theorie des elektrischen Rückstandes in der Leidener Flasche, Ann. Phys. Chem. **167**, 56 (1854).

[35] G. Williams and D. C. Watts, Non-symmetrical dielectric relaxation behaviour arising from a simple empirical decay function, Transac. Faraday Society **66**, 80 (1970).

[36] C. P. Lindsey and G. D. Patterson, Detailed comparison of the Williams-Watts and Cole-Davidson functions, J. Chem. Phys. **73**, 3348 (1980).

[37] J. G. Berberian and R. H. Cole, Approach to glassy behavior of dielectric relaxation in 3-bromopentane from 298 to 107 K, J. Chem. Phys. **84**, 6921 (1986).

[38] N. Verdal, T. J. Udovic, V. Stavila,W. S. Tang, J. J. Rush, and A. V. Skripov, Anion reorientations in the superionic conducting phase of $Na_2B_{12}H$, J. Phys. Chem. C **118**, 17483 (2014).

[39] N. Verdal, M. R. Hartman, T. Jenkins, D. J. DeVries, J. J. Rush, and T. J. Udovic, Reorientational dynamics of $NaBH_4$ and KBH_4, J. Phys. Chem. C **114**, 10027 (2010).

[40] M. Bée, *Quasielastic Neutron Scattering, Principles and Application in Solid State Chemistry, Biology and Materials Science* (Adam Hilger, Bristol and Philadelphia, 1988).

[41] R. Hempelmann, *Quasielastic Neutron Scattering and Solid State Diffusion* (Clarendon Press, Oxford, 2000).